AALBORG UNIVERSITY
DENMARK

Environmental effects on the cohesive laws of the composite bonded joints

Abdel-Monsef, S.; Renart, J.; Carreras, L.; Maimí, P.; Turon, A.

Link to publication from Aalborg University

Environmental effects on the cohesive laws of the composite bonded joints

S. Abdel-Monsef [b], J. Renart [a,1], L. Carreras [c], P. Maimí [a], A. Turon [a,*]

[a] *AMADE, Polytechnic School, University of Girona, Campus Montilivi s/n, 17003 Girona, Spain*
[b] *Structural Engineering Dept., Faculty of Engineering, Zagazig University, P.O. Box 44519, Zagazig, Sharkia, Egypt*
[c] *Dept. of Materials and Production, Aalborg University, Fibigerstraede 16, DK-9220, Aalborg East, Denmark*

ARTICLE INFO

ABSTRACT

This paper investigates the effect of environmental conditions on the cohesive law of composite bonded joints under mode I and mode II loadings. An inverse method recently developed by the authors has been used to extract the cohesive stress-separation relation from the experimental load–displacement curve without considering a predefined shape of the cohesive law. Two types of adhesively composite bonded joints were tested at three different temperatures, −55 °C, room temperature and 80 °C and two ageing conditions (wet-aged and non-aged) for four years. The shape and parameters of the cohesive law have been compared among the different ageing and test temperature conditions. The shape of the cohesive law that best fits the experimental results has been identified depending on the loading mode, test temperature and environmental conditions.

1. Introduction

The environmental factors, especially temperature and humidity, degrade the mechanical properties of composite bonded joints [1,2]. The exposure to high temperatures affects both chemical and physical properties of the adhesive changing the bond strength [3]. Furthermore, the existence of moisture in composite bonded joints may affect the interface between adherent and adhesive in addition to the physical and chemical properties of the adhesive [4]. Moreover, the exposure to a combination of moisture and temperature leads to more damage than to an individual condition [5–7].

Several researches studied the effect of environmental degradation and weathering on the fracture response of composites [1,2,4–13]. Banea et al. [14] investigated the influence of temperature on the fracture response of adhesives using two different test configurations: tensile and mode I Double Cantilever Beam (DCB) tests. They found that the ductility of the adhesive increases with the temperature. Moreover, the exposure to wet ageing causes great degradation of the bonded joint strength [15–18]. Fernandes et al. [2] investigated the influence of moisture on the fracture behaviour of composite bonded joints. The specimens were made with carbon-epoxy laminates and structural adhesive (Araldite 2015) using the double cantilever beam test and subjected to ageing conditions (55% and 75% of relative humidity (RH) and immersion in distilled water (IW)) for four months. They noticed

that the increase of the relative humidity causes more degradation on the mechanical properties of the adhesive joints.

Cohesive zone modelling is a powerful tool to simulate the mechanical behaviour of composite bonded joints. However, there is a limited number of studies devoted to investigate the effect of environmental conditions on the cohesive law. Environmental changes not only affect the fracture toughness and bond strength but also the cohesive law shape [1,2,19]. Gustafson and Waas [10] built a procedure to define the parameters of a cohesive bilinear law over the temperature range of 20 to 350 °C. For mode I, they used two different methodologies to obtain the fracture toughness from DCB tests: the area data reduction method and an inverse FE analysis. The strength of the bonded joint was determined via an specialized button peel stress test. For mode II, the fracture toughness was determined using the ENF test configuration in combination with the compliance calibration data reduction method, while the cohesive strength was measured using the single lap joint test. The interdependence between mode II fracture toughness and strength was accounted by a surrogate model based mapping technique. Banea et al. [20] studied the effect of elevated temperature on the fracture toughness. They simulated a DCB test with a bilinear cohesive law to predict the load–displacement curves as a function of the temperature. The sensitivity of the DCB output to the cohesive parameters was also analysed. They also used a bilinear cohesive law to predict the load–displacement results of an ENF test at different

---

temperatures [21]. Fernandes et al. [1] used a trapezoidal cohesive law to study the fracture behaviour of adhesively bonded joints under different temperatures (0 °C, 25 °C (room condition) and 50 °C) for pure modes I and II.

Through the studies mentioned above, it is still an open issue to obtain the cohesive law of composite bonded joints under different temperatures. The few existing studies used predefined shapes (e.g. linear, triangular, parabolic, exponential and trapezoidal shapes) to predict the cohesive parameters such as the maximum stress in each fracture mode and the fracture toughness of adhesives, which are particularly sensitive to temperature [14]. However, the shape of the cohesive law contains information of the physical damage processes underlying at the micro-scale and it is essential for accurate mechanical response predictions of the bonded joint.

In the current work, the effect of both temperature and ageing on the cohesive laws of composite bonded joints under mode I and mode II loading conditions is investigated using specimens made with two different types of adhesives. For this purpose, Double Cantilever Beam (DCB) and End Load Split (ELS) tests were carried out at different temperatures (−55 °C, Room Temperature (RT) and 80 °C) after different ageing conditions (non-aged and wet-aged) for four years. An efficient method to extract the full shape of the cohesive law from the experimental load–displacement curves was used. Finally, the dependence of the Cohesive Law (CL) shape and parameters on the environmental effects is investigated.

2. Methodology

2.1. Experimental test campaign

In order to investigate the effect of environmental conditioning on the response of composite bonded joints, an experimental test campaign was carried out using the DCB test [22] for mode I and the ELS test [23] for mode II, respectively. All the tests were carried out at AMADE laboratory of the University of Girona, which is ISO17025 and NADCAP (National Aerospace and Defense Contractors Accreditation Program) accredited for testing non-metallic materials.

Two different bonded joint configurations (A1 and A2) were manufactured using two different epoxy adhesive films and the same adherend. The adherends were made of a carbon tape epoxy prepreg multidirectional balanced panels $[0/0/+45/−45/+45/−45]_S$ produced in an autoclave. The adhesives were rigid epoxy films embedding a Mat/Polyester carrier. The first adhesive film is from Cytec Engineered Materials with a glass transition temperature Tg ≈ 140 °C, while the second adhesive is from Henkel with Tg ≈ 122 °C. Surface conditioning of the adherends for bonding was conducted by abrasion accompanied by solvent cleaning. Then, the specimens were cured in an autoclave. For reasons of confidentiality, the commercial names of the adherend and adhesives are not listed. After the specimens were prepared, they were grouped according to the exposure to the ageing process (wet-aged and non-aged) and the temperature of testing (−55 °C, RT, 80 °C), as outlined in Table 1 where the label "*/*/W" refers to the wet-aged specimens while "*/*/L" refers to the non-aged specimens.

The wet-aged specimens were stored in an environmental chamber being exposed to accelerated ageing (Temperature of 70 °C and 85% RH). Fig. 1 shows the moisture uptake curve for A1 and A2 specimens during four years to simulate long-term exposure to environmental changes. It should be noted that the relative moisture content is calculated for the whole specimen where the moisture will be taken up by both the adhesive and the composite adherends. The non-aged specimens were stored in the laboratory under controlled conditions at RT and tested together with the wet-aged specimens, after four years from the manufacturing time.

Mode I specimens were 25 mm wide and 4.4 mm thick. The wet-aged specimens were 210 mm long, whereas the non-aged specimens were 185 mm long. Mode II specimens were 25 mm wide,

Table 1
Specimen configurations tested.

ID	Adhesive	Test temperature	Conditioning Before test
A1/RT/L		RT	
A1/80/L	A1	80 °C	non-aged[a]
A1/-55/L		−55 °C	
A1/RT/W		RT	
A1/80/W	A1	80 °C	wet-aged[b]
A1/-55/W		−55 °C	
A2/RT/L		RT	
A2/80/L	A2	80 °C	non-aged[a]
A2/-55/L		−55 °C	
A2/RT/W		RT	
A2/80/W	A2	80 °C	wet-aged[b]
A2/-55/W		−55 °C	

[a] The specimens were stored in laboratory conditions at room temperature for four years.
[b] The specimens were aged at 70 °C and a relative humidity of 85% in a conditioning chamber for four years.
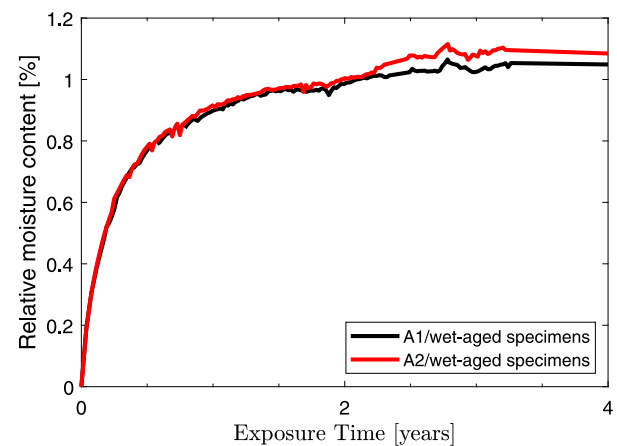

Fig. 1. Moisture uptake curves of the wet-aged specimens.

4.60 mm thick and 210 mm long. The thickness of the adhesive layer was 0.22 ± 0.02 mm in the case of the non-aged specimens and 0.3 ± 0.015 mm in the wet-aged specimens. This difference in the adhesive thickness is due to the moisture absorption in the case of the wet-aged specimens. For all specimens, a doubled layer of PTFE (Polytetrafluoroethylene) insert was used to trigger interface debonding and introduce an artificial crack length. In the case of mode I, the length of the insert was 75 mm and 60 mm in the wet-aged and non-aged specimens, respectively. In mode II specimens, the insert was 70 mm long.

With the aim of avoiding unstable crack growth from the insert, a pre-crack test was made following ISO25217 [22] and ISO15114 [23] for mode I and mode II specimens, respectively. The pre-crack propagation was set to a minimum length of 2 mm for DCB specimens and 5 mm for ELS specimens. After the pre-crack tests, the crack length was measured using an optical microscope. Further details of the tests may be found in [24,25].

Both DCB and ELS tests were carried out under displacement control at a constant displacement rate (5 mm/min and 1 mm/min for the loading process of the DCB and ELS tests, respectively) in an electromechanical MTS testing machine equipped with a 10 kN load cell. For each batch listed in Table 1, five specimens were prepared to be tested. The specimens were tested at three different temperatures (−55 °C, RT and 80 °C). The wet-aged specimens were moved from the environmental chamber to a temperature release box until the specimen's temperature reached the surrounding temperature. Then, the specimen was immediately tested. Changes in moisture content
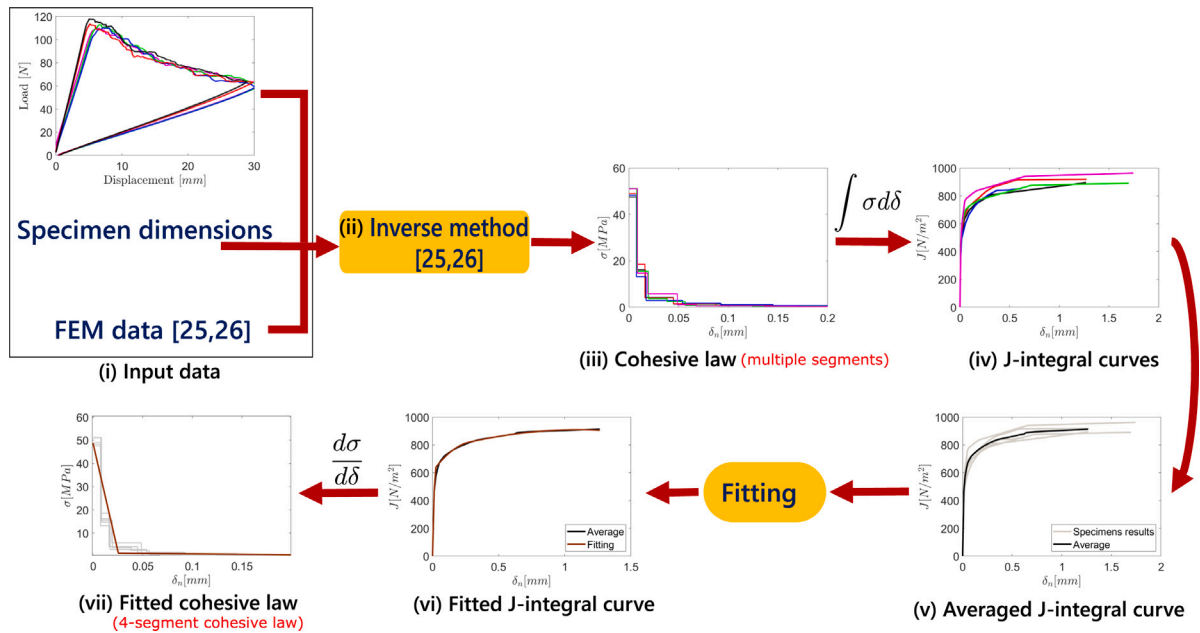
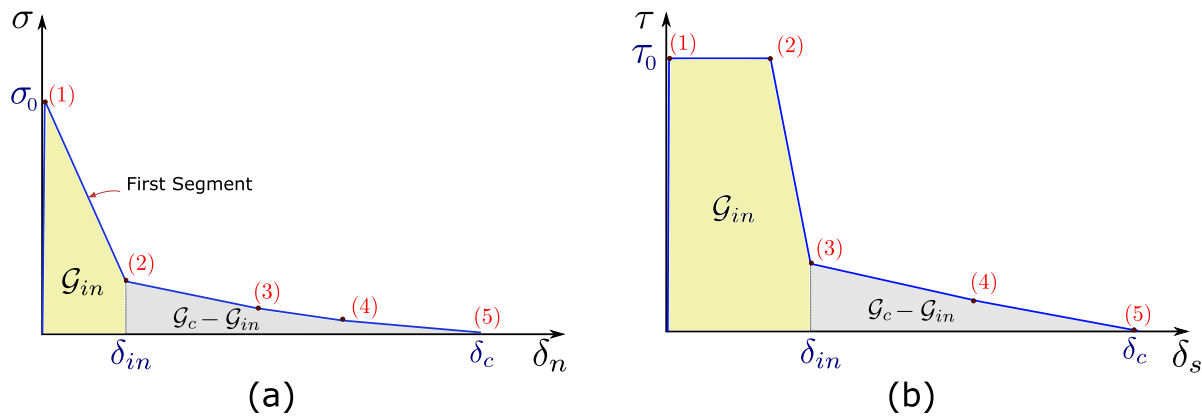**Fig. 2.** A sketch of a procedure to obtain the smoothed cohesive laws.

Fig. 3. A sketch of a multilinear cohesive law with four line segments to fit the obtained J-integral from (a) DCB and (b) ELS tests.

during this process were monitored by comparing the weight of the specimens after removing them from the environmental chamber and just before testing. The variance in weight was ensured to be less than the tolerance of $\pm 0.01\%$ [25].

To measure the temperature of the coupon specimen during the test, a thermocouple attached to the upper face of the specimen tested was used. The load data obtained from the load cell was synchronized together with the measured displacement and temperature and acquired in real-time using a data acquisition system QuantumX.

2.2. Data reduction methods

To investigate the influence that the environmental conditions have on the shape of CL, the inverse method developed in [26,27] was used. The method extracts the cohesive laws from the load–displacement curves obtained from both DCB and ELS tests carried out in [24, 25]. In order to use the inverse method, the finite element software (ABAQUS [28]) to obtain the non-dimensional parameters (referred as FEM data) found in [26,27] was used. The DCB and ELS problems were modelled using the parametric finite element model constructed in [26,27] using 2D plane strain CPE4I elements with squared element sizes of 0.1 mm. A stress profile was applied to the element edges located at the interface to act as the adhesive interface. Consequently,

the FEM data (stress intensity factors, opening/shear displacements and vertical displacements at the loading point) were obtained due to unitary loads [26,27]. To obtain the cohesive laws, the procedure shown in Fig. 2 was used. The input data are selected points of the load–displacement curve (between the onset of non-linearity and crack propagation [26]), the geometry of the specimen and the FEM data. Then, the relation of J-integral versus displacement jump was obtained by numerical integration of the extracted cohesive law. To simplify the comparison and to be useable in a finite element framework, the averaged J-integral vs displacement jump curve was fitted into a four segments geometrical function. Finally, the derivation of the fitted J-integral curve results in the four-segments CL shown in Fig. 3.

For clarity, the first point of the input data should be carefully selected where the load–displacement curve loses its linearity (the onset of the nonlinear stage). The authors considered this point when the crack has initiated across the entire specimen width. The used inverse method is limited to a 2D plane strain problem, which does not count the effect of the specimen's width on the crack initiation. On the other hand, the selection of the last point is in some way arbitrary, because it is challenging to predefine this point where the steady-state has been reached. Nevertheless, if this does not occur we can modify the selection by adding another point until the fracture process zone is totally developed (i.e. steady-state).

(a) A1 (DCB)

(b) A2 (DCB)

(c) A1 (ELS)

(d) A2 (ELS)
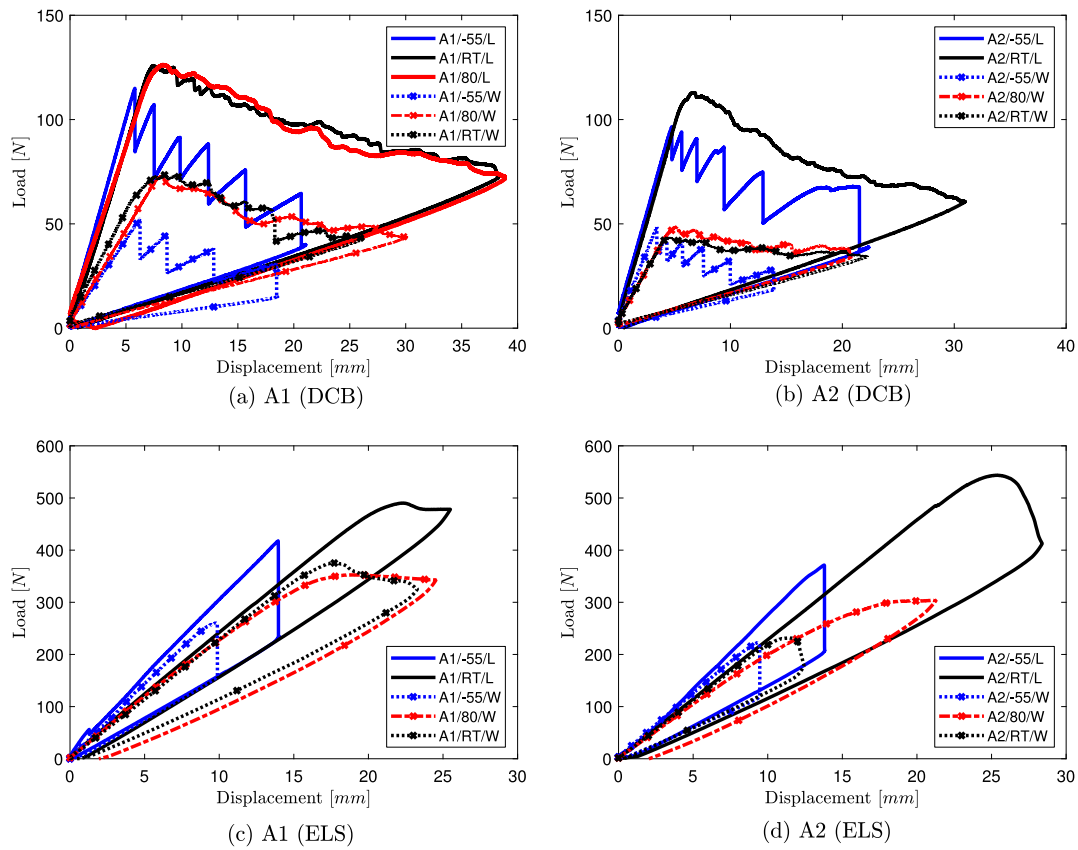
Fig. 4. Load–displacement curves of DCB and ELS tests for A1 and A2 configurations under different environmental conditions (L: non-aged and W: wet-aged).

(a) A1/RT/L

(b) A1/80/L

(c) A1/-55/L

(d) Cohesive laws

Fig. 5. DCB results of the non-aged A1 specimens: J-integral curves obtained from (a) RT specimens, (b) 80 °C and (c) −55 °C, and (d) the cohesive law obtained from the fitting of the average J-integral curves. δ_n is the normal opening displacement.

(a) A2/RT/L

(c) A2/-55/L

(d) Cohesive laws

Fig. 6. DCB results of the non-aged A2 specimens: J-integral curves obtained from (a) RT specimens, and (b) −55 °C, and (c) the cohesive law obtained from the fitting of the average J-integral curves. δ_n is the normal opening displacement.

(a) A1/RT/W

(b) A1/80/W

(c) A1/-55/W

(d) Cohesive laws

Fig. 7. DCB results of the wet-aged A1 specimens: J-integral curves obtained from (a) RT specimens, (b) 80 °C and (c) −55 °C, and (d) the cohesive law obtained from the fitting of the average J-integral curves. δ_n is the normal opening displacement.

(a) A2/RT/W

(b) A2/80/W
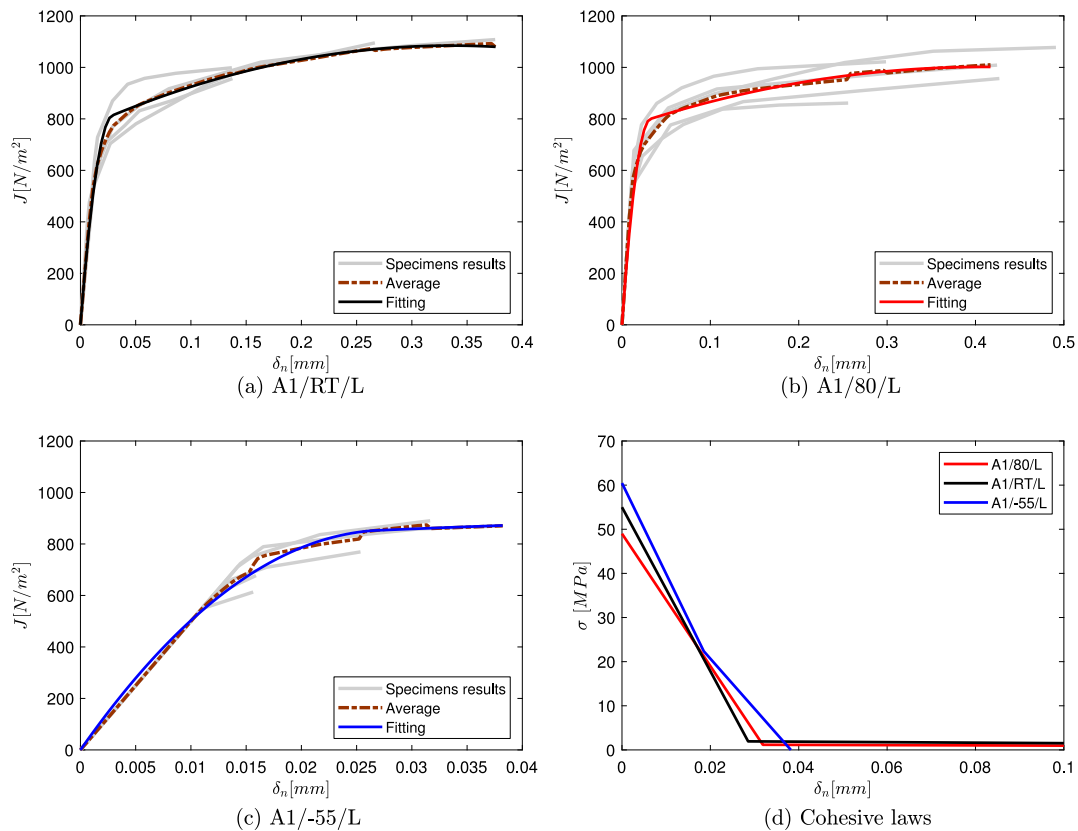
(c) A2/-55/W

(d) Cohesive laws

Fig. 8. DCB results of the wet-aged A2 specimens: J-integral curves obtained from (a) RT specimens, (b) 80 °C and (c) −55 °C, and (d) the cohesive law obtained from the fitting of the average J-integral curves. δ_n is the normal opening displacement.
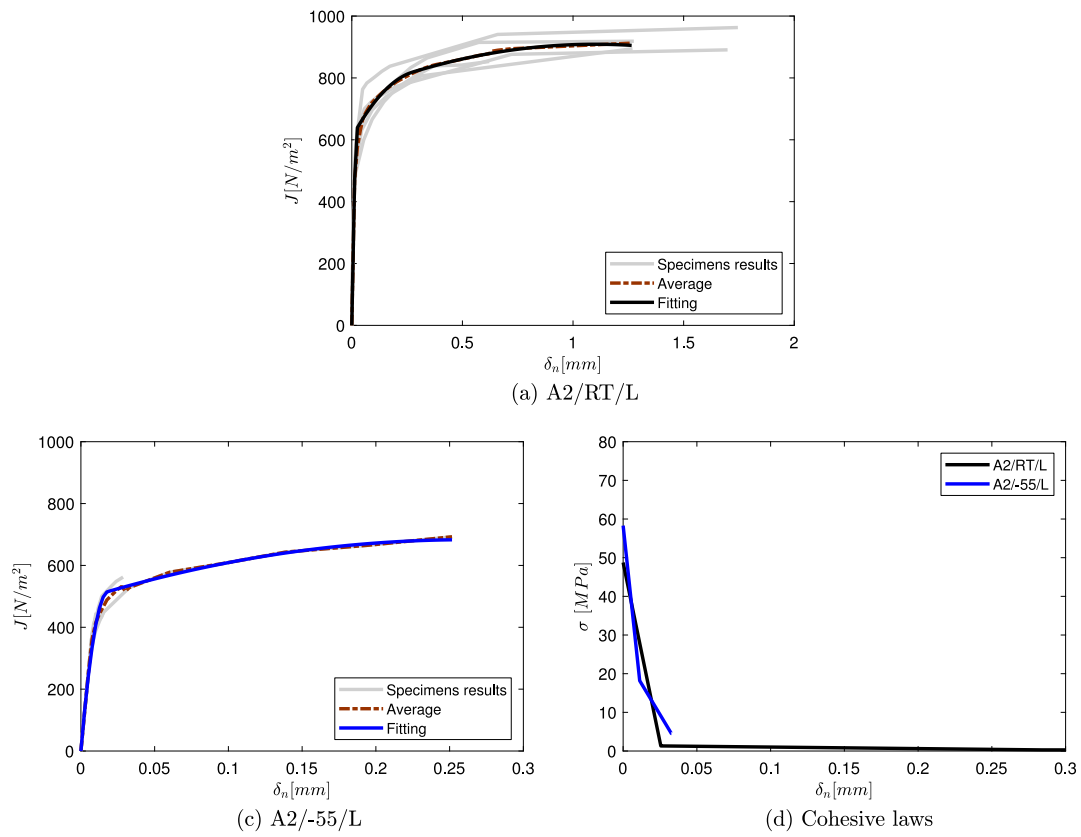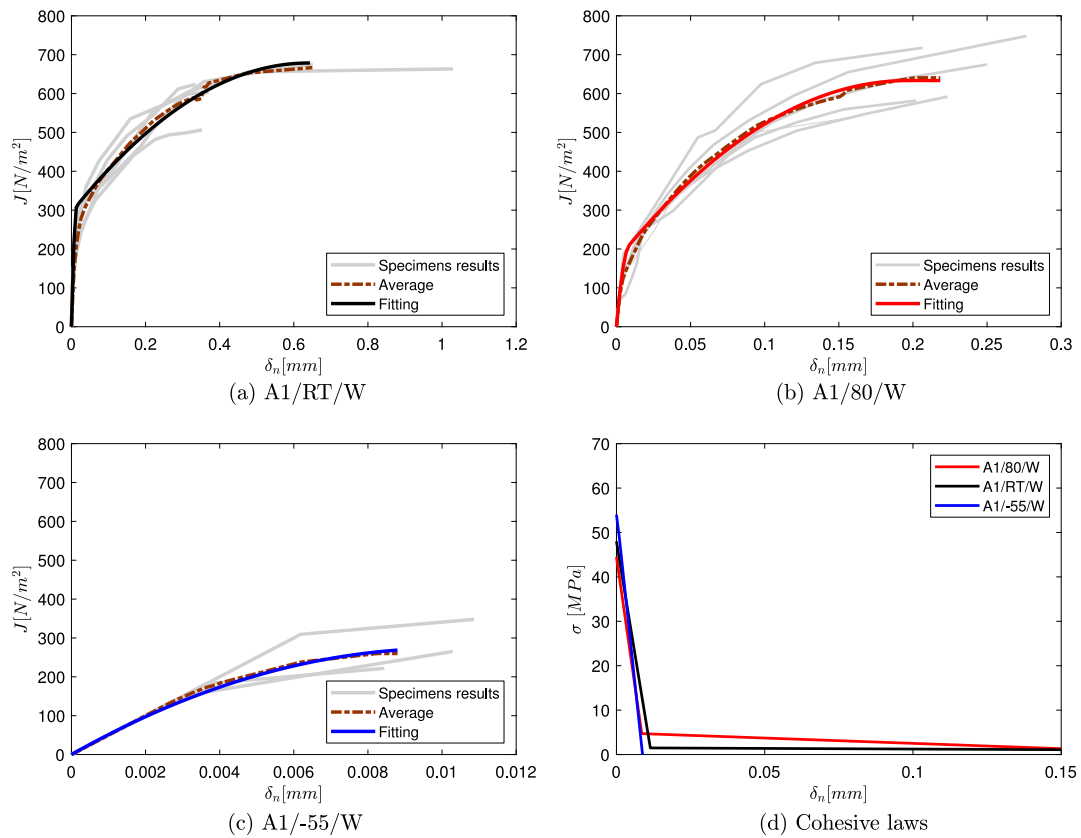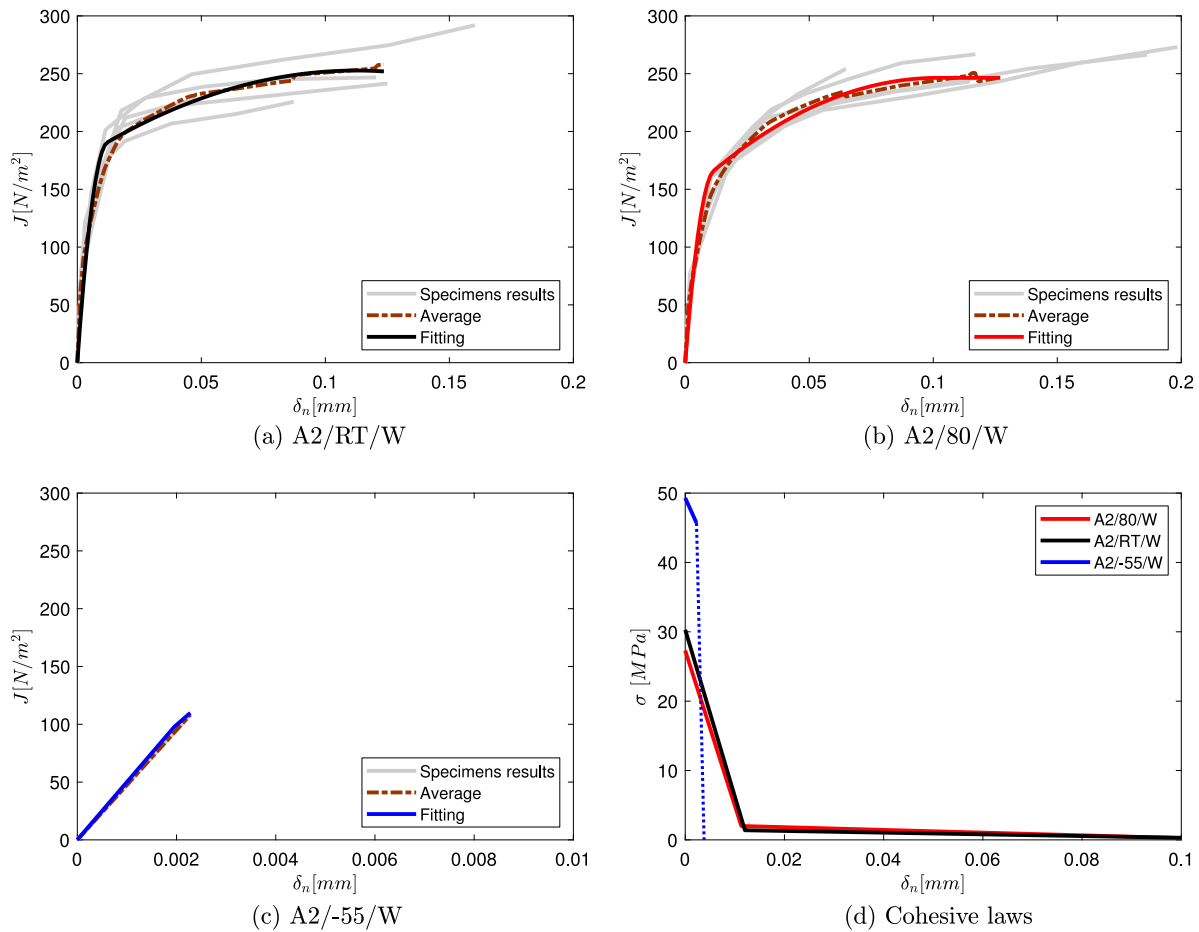
The critical energy release rate, $\mathcal{G}_c$, is the maximum J-integral value (i.e. the total area under the fitted cohesive law). $\mathcal{G}_{in}$ defines only the area under the first segment of CL (see Fig. 3) and does not refer to crack initiation values. Thus, in the current work, $\mathcal{G}_{in}$ does not define the material elastic limit where damage starts to develop. It must be mentioned $\mathcal{G}_{in}$ does not refer to the initiation energy or the onset energy. σ_0 and τ_0 are the maximum cohesive stress values for mode I and mode II, respectively. In the displacement axis, the subscripts $(\bullet)_n$ and $(\bullet)_s$ refer to mode I and mode II, respectively.

3. Results

On the aim of studying the effect of environmental changes on the shape of cohesive laws of composite bonded joints, the cohesive laws from the load–displacement curves from the DCB and ELS tests carried out in [24,25] with the method presented in [26,27] were obtained. In the case of the DCB configuration, the used load–displacement curve is the superposition of the load–displacement curves obtained from the pre-cracking and the fracture test. Fig. 4 shows a representative load–displacement curve for each environmental condition (testing temperature and thermal ageing process) and adhesive material (A1 and A2) for both DCB and ELS tests.

Figs. 5 and 6 show the resulting J-integral versus the displacement jump curves of the non-aged DCB specimens for each test temperature and the obtained cohesive laws. The non-aged specimens results evidence the effect of temperature: high temperature has a small effect on the cohesive laws. This can also be observed from the similar behaviour in the corresponding load–displacement curves shown in

Fig. 4-a (A1/RT/L and A1/80/L). On the contrary, exposing the specimens to low temperature (−55 °C) has a significant influence on cohesive behaviour. As shown in Figs. 5 and 6, a hardening behaviour was observed for the tests performed under low-temperature. Short opening critical displacements were obtained (around 0.04 mm for specimens A1/-55/L and A2/-55/L). However, the first part of the cohesive laws up to an opening displacement around 0.04 mm, is very similar for all the configurations tested.

Figs. 7 and 8 show the results of the wet-aged DCB specimens for the configurations A1 and A2, respectively. Although high temperature slightly affects the fracture toughness of DCB specimens, either non-aged or wet-aged, it changes the shape of the cohesive laws. Freezing temperatures increase the brittleness behaviour which affects the last part of the cohesive law as shown in Figs. 7-d and 8-d for A1 and A2 specimens, respectively.

Concerning the −55 °C DCB tests, incomplete cohesive laws were obtained because of the stick–slip crack growth behaviour observed in Fig. 4. Consequently, the cohesive laws were extracted from the load–displacement curve of the −55 °C DCB specimens until the first peak load because it is not possible to fit the sudden drop of the load using the inverse method [24]. However, it is possible to complete the last segment of the cohesive law in the case of −55 °C tests using the fracture toughness value obtained from other data reduction methods found in [24] (see the blue dash line in Fig. 8-d).

Regarding the environmental effect on mode II, both J-integral curves and the associated cohesive laws were plotted in Figs. 9 to 12. Figs. 9 and 10 show the results of the non-aged ELS specimens for the A1 and A2 configurations, respectively.
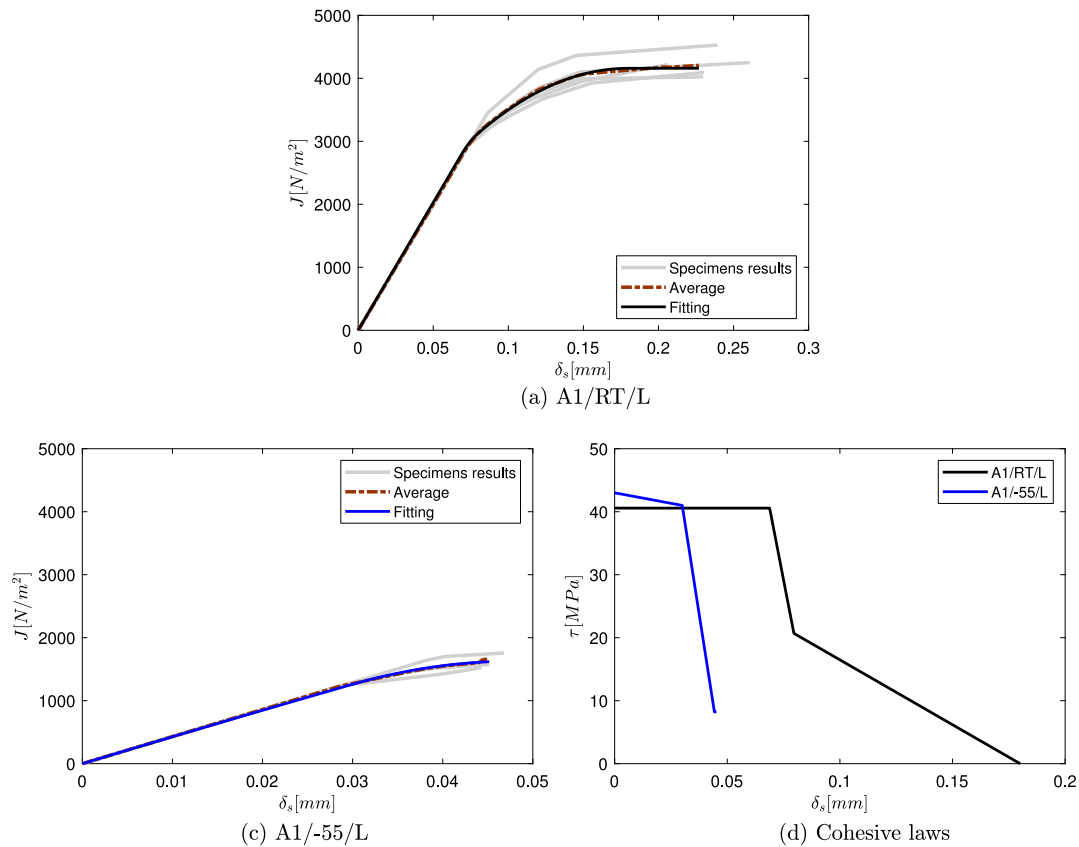
(a) A1/RT/L

(c) A1/-55/L

(d) Cohesive laws

Fig. 9. ELS results of the non-aged A1 specimens: J-integral curves obtained from (a) RT specimens and (b) −55 °C, and (c) the cohesive law obtained from the fitting of the average J-integral curves. δ_n is the normal opening displacement.

For wet-aged ELS specimens, Figs. 11 and 12 show the obtained J-integral curves using the inverse method and the corresponding cohesive laws of A1 and A2 configurations, respectively, tested at temperatures −55 °C, RT and 80 °C. Both high and low temperatures have a notable effect on the cohesive law shape of the wet-aged ELS specimens. Testing at high temperature has a slight effect on the fracture toughness of A1 specimens; but, it causes a considerable increase in the fracture toughness of A2 specimens.

In some cases, the CL was not entirely obtained (i.e. cohesive shear stress does not reached zero) for the specimens exposed to 80 °C and −55 °C and tested under mode II conditions. This is because of the effect of the temperature on the behaviour of composite bonded joints. On the one hand, high temperature increases the ductility of the adhesive causing a large damage process zone that can only fully develop if the propagation region is large enough. On the other hand, freezing temperature increases the brittleness and leads to unstable crack propagation.

The effect of the testing temperature on the parameters $\mathcal{G}_c$, $\mathcal{G}_{in}$ and δ_{in} is summarized in Figs. 13(a) and 13(b) for the DCB and ELS results, respectively. In addition, the effect of the ageing process on those parameters and the maximum cohesive stresses (σ_0 and τ_0) is shown in Fig. 14. The obtained results at temperature T were normalized with the room temperature result for each case of the non-aged and the wet-aged specimens.

$$\hat{\mathcal{R}^{(T)}} = \frac{\mathcal{R}^{(T)}}{\mathcal{R}^{(T=RT)}} \tag{1}$$

where $\mathcal{R}$ refers to one of the parameters $\mathcal{G}_c$, $\mathcal{G}_{in}$, σ_0, τ_0 and δ_{in}.

Finally, the fractured surfaces on the bonded area found in [24,25], are summarized in Fig. 15.

4. Discussion

It is worth mentioning that previous studies to this work used specimens exposed to an ageing process for a time less than one year. It can be seen in Fig. 1, that in the case of the specimens being tested in this work, the moisture uptake cannot be considered stabilized before, at least, three years of ageing exposure.

From the analysis of the load–displacement response, the J-integral curves and the associated cohesive laws for both adhesive types A1 and A2, it can be asserted that environmental factors affect the properties of the composite bonded joints, in agreement with what was discussed in [1,2,13,20,29–31].

4.1. Effect of temperature/ageing on the cohesive law shape

To sum up the observed effects that environmental conditions have on the shape of the cohesive law, Fig. 16 shows a schematic sketch using four-segment cohesive laws for Mode I and Mode II.

Temperature has a significant effect on the fracture behaviour of the composite bonded joints. Adhesives exposed to sub-zero temperatures are expected to behave as brittle adhesives [9] which causes unstable crack propagation (stick–slip behaviour in the case of mode I [32] or sudden failure in the case of mode II [33]). This behaviour observed in the obtained cohesive laws of the specimens tested at −55 °C. In the case of mode I, since low temperatures lead to brittle behaviour of the adhesive, the strain to failure is reduced [9] (see Fig. 16.a). The slope of the CL of the −55 °C specimens is close to that of the first segment of the RT cohesive laws, with complete failure reached at very low opening displacement. Although a cohesive failure was observed in the case of mode I, the stick–slip behaviour prevented the fitting of the whole load–displacement curve and thus, acquiring the full cohesive law. For mode II, the shape of the −55 °C CL has an initial

(a) A2/RT/L

(c) A2/-55/L

(d) Cohesive laws

Fig. 10. ELS results of the non-aged A2 specimens: J-integral curves obtained from (a) RT specimens and (b) −55 °C, and (c) the cohesive law obtained from the fitting of the average J-integral curves. δ_n is the normal opening displacement.

(a) A1/RT/W

(b) A1/80/W

(c) A1/-55/W

(d) Cohesive laws

Fig. 11. ELS results of the wet-aged A1 specimens: J-integral curves obtained from (a) RT specimens, (b) 80 °C and (c) −55 °C, and (d) the cohesive law obtained from the fitting of the average J-integral curves. δ_n is the normal opening displacement.
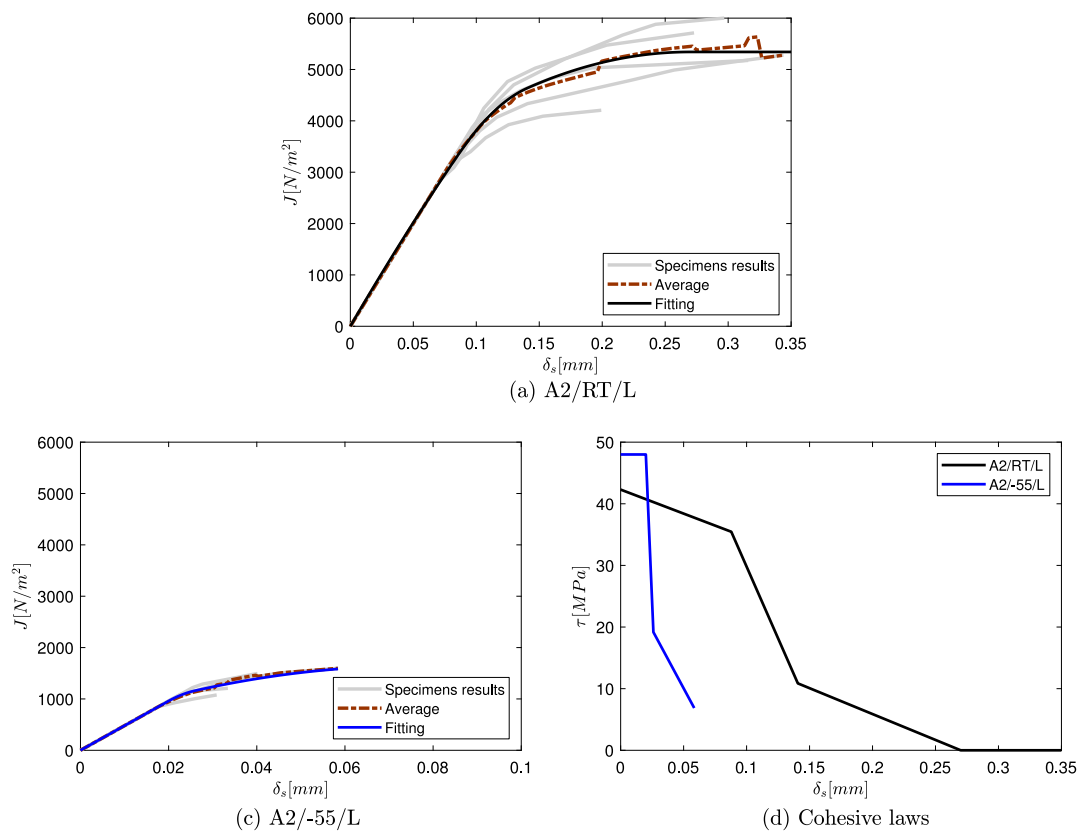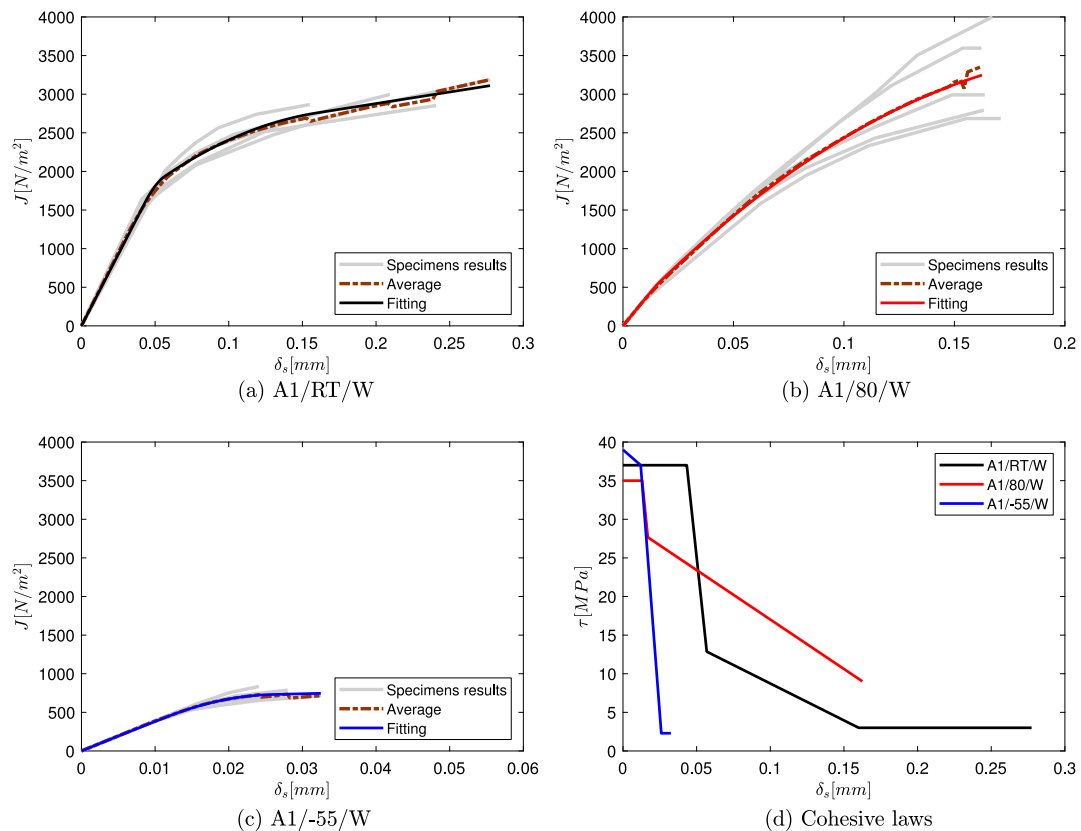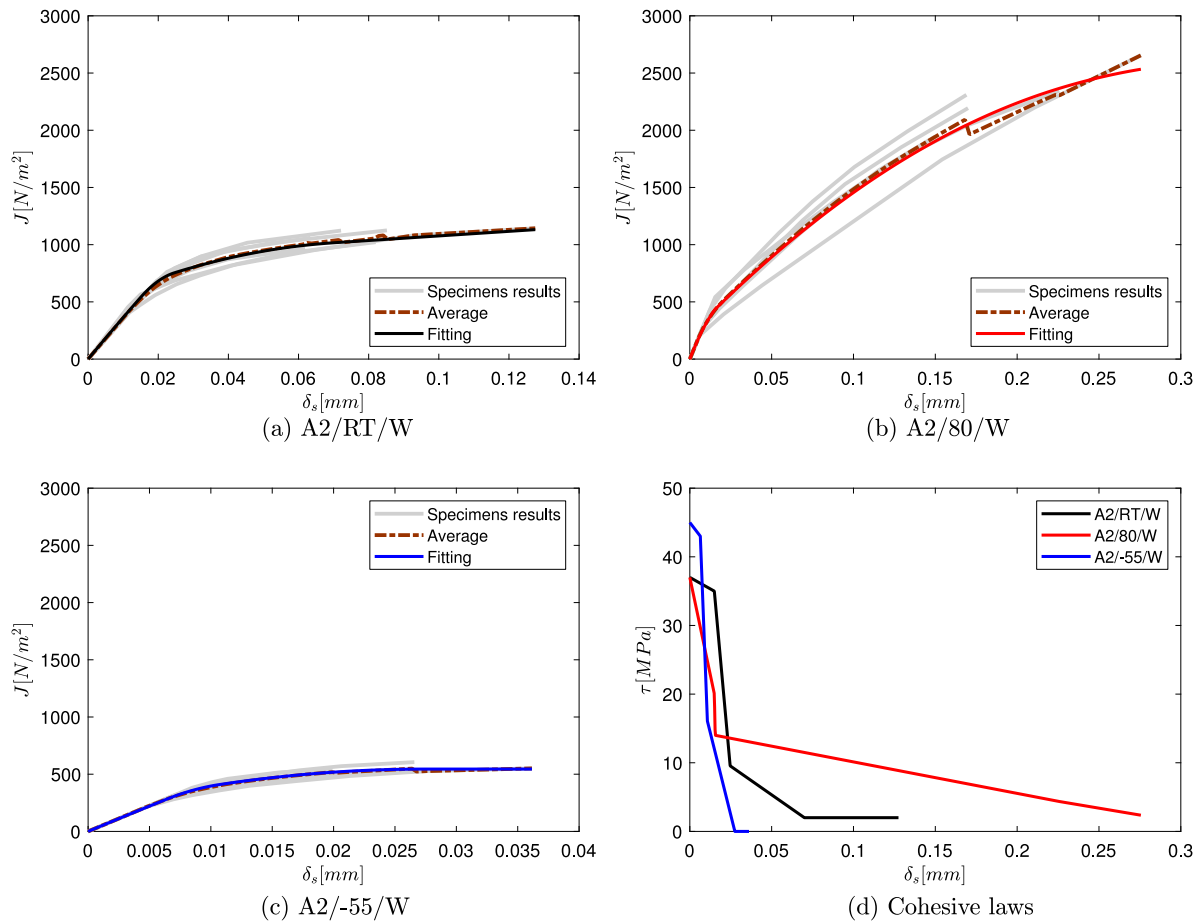
Fig. 12. ELS results of the wet-aged A2 specimens: J-integral curves obtained from (a) RT specimens, (b) 80 °C and (c) −55 °C, and (d) the cohesive law obtained from the fitting of the average J-integral curves. δ_n is the normal opening displacement.
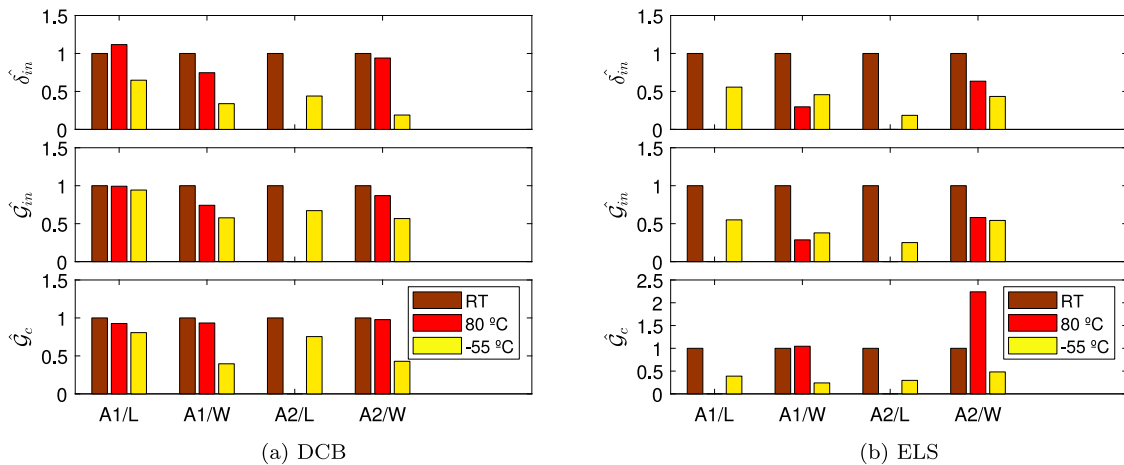

Fig. 13. The summary of DCB and ELS test results normalized by the result at each RT of each configuration. (L: non-aged and W: wet-aged)

plateau, likewise the first segment of RT laws. However, the drop in stress is produced at comparatively lower displacement jump, causing a significant reduction in the cohesive law area (see Fig. 16.b). It can be observed in Fig. 15 that the crack propagation path migrates to the weakest interface between the adhesive and the adherend substrate. This caused a more brittle behaviour and a premature failure (incomplete cohesive law was measured). In fact, the obtained cohesive law defines the interface property and does not correspond to the adhesive property.

Conversely, high temperature increases the ductility of the adhesive. In the case of the adhesives tested, which are thermosets, temperature below the Tg has small on the fracture behaviour. It can be observed in Fig. 15 that the obtained fracture surfaces of the specimens tested at 80 °C are similar to the RT ones. The mode I cohesive laws of the specimens tested at RT and 80 °C are close in shape and area under the curves (see Fig. 16.a). However, for Mode II, despite the similarity between RT fractured surfaces and those tested at 80 °C, there is a significant effect of high temperature on the shape of cohesive law. This effect is attributed to a longer and wider tail of the cohesive law
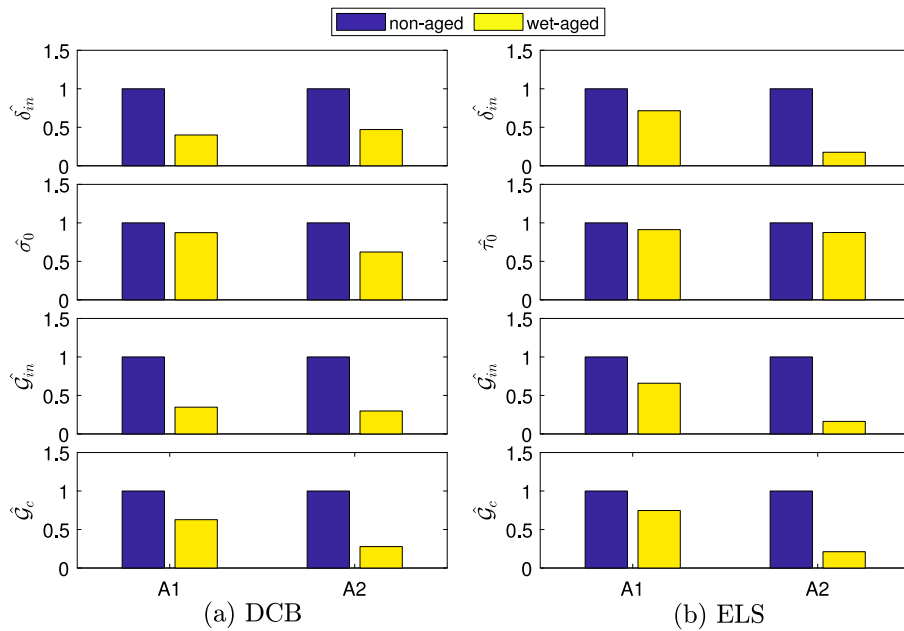
Fig. 14. The summary of the non-aged and wet-aged specimens normalized with the non-aged case.
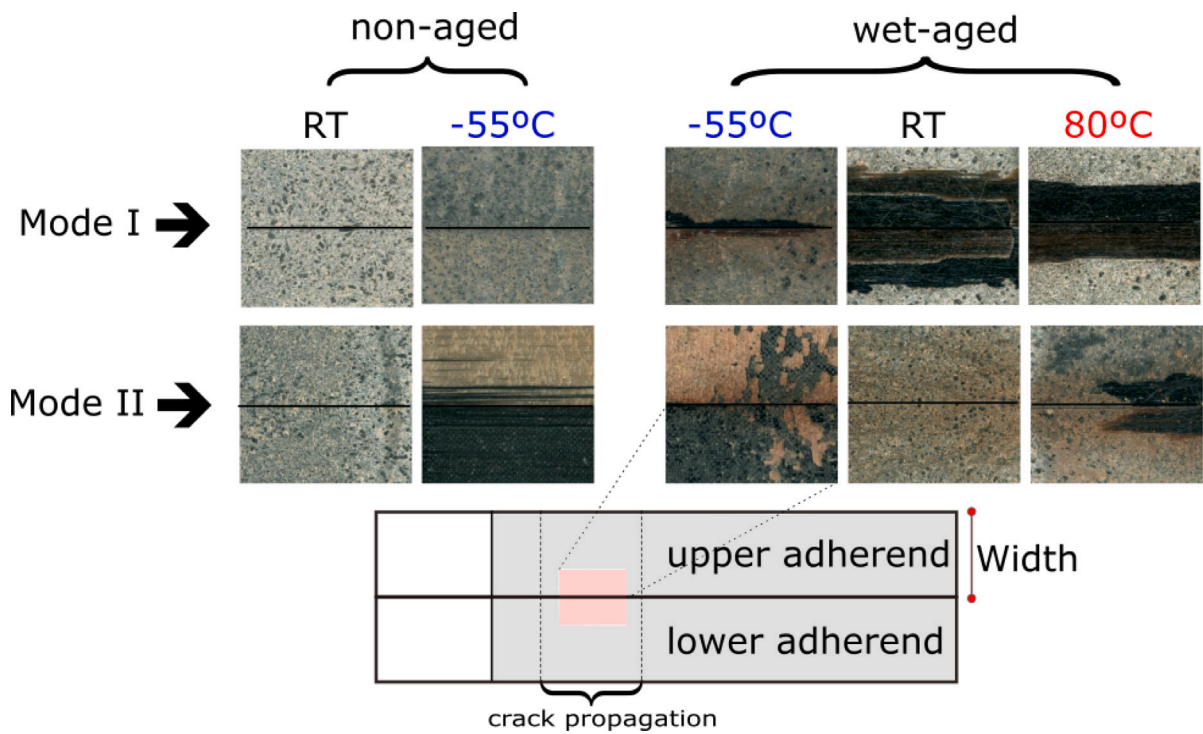

Fig. 15. Summary of the fractured surface pictures of the tested DCB and ELS specimens found in [24,25] for A1 bonded joints.

(see Fig. 16.b). Moreover, high-temperature increases the length of the fracture process zone causing that its full formation is not reached within the propagation length limits. The authors suggest increased ductility on the tail instead of the first segment because the exposure time is too long in mode II tests.

To understand how four years of ageing exposure time affects the shape of the cohesive law, the wet-aged and the non-aged cohesive laws can be compared. The ageing process had a slight effect on

the shape of the cohesive law, but it significantly reduced the area under the cohesive law (see Figs. 16.c and 16.d), especially for the A2 adhesive where the curing temperature is closer to the Tg. This reduction in the area can be related to the observed change in the failure mode from a purely cohesive mode to either mixed cohesive-interlaminar or mixed cohesive-interfacial in the wet-aged specimens subjected to a long ageing process in the climatic chamber. As can be observed in Fig. 15, the failure path in the wet-aged bonded joints in
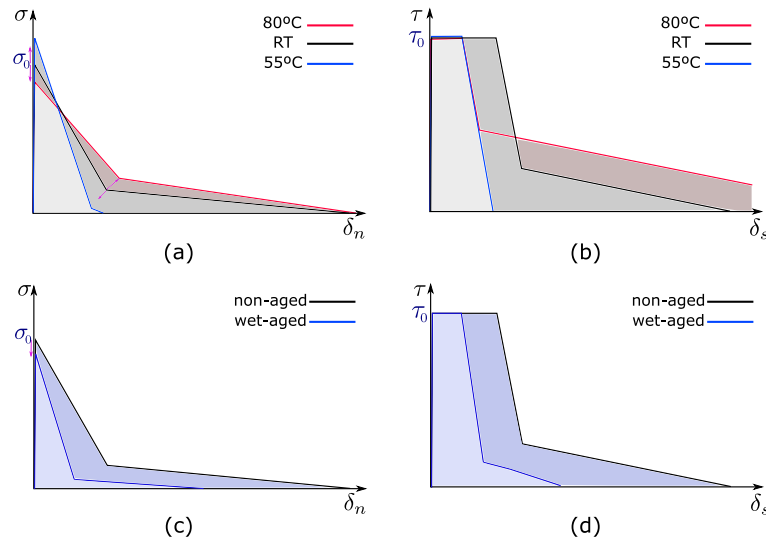
σ

σ_0

80ºC
RT
55ºC

δ_n

(a)

τ

τ_0

80ºC
RT
55ºC

δ_s

(b)

σ

σ_0

non-aged
wet-aged

δ_n

(c)

τ

τ_0

non-aged
wet-aged

δ_s

(d)

Fig. 16. Schematic illustration of environmental conditions influences on the simplified cohesive laws.

mode I becomes predominantly interlaminar in the composite, which is driven by the properties of the adherend (i.e. the epoxy matrix in the carbon fibre tape pre-preg). On the other hand, the failure path becomes predominantly interfacial in mode II which direct the crack propagation to the weakest path between the adhesive and the adherend causing adhesive failure. Therefore, the measured cohesive law represents some form of average across the mixed failure type to define the interface property and does not correspond to the adhesive property. The existence of moisture in composite bonded joints may affect the interface between the adherend and the adhesive in addition to the physical and chemical properties of the adhesive itself [4]. For the wet-aged specimens tested at −55 °C, freezing temperature add more damage to that caused solely by ageing because freezing the water absorbed by the matrix can create cracks in the material volume and lead to premature failure.

4.2. Effect of temperature/ageing on the cohesive law parameters

Freezing temperatures cause the failure behaviour to move from a ductile to a brittle. This can be noticed in the load–displacement curves (see Fig. 4). This effect can also be shown in Fig. 13, where an important reduction, between 35% and 50% is observed in the values of δ_{in} from the specimens tested at −55 °C in comparison with RT. Furthermore, $\mathcal{G}_{in}$ constitutes the majority of the area under the cohesive laws ($\mathcal{G}_{in}/\mathcal{G}_c \geq 60\%$) in the case of testing at −55 °C. In addition, different crack propagation and stability were noticed. In the DCB tests, unstable propagation occurs when specimens are exposed to −55 °C, while freezing temperatures cause a sudden failure in the ELS tests. With the aim of obtaining stable crack propagation, the a_0/L ratio was increased from 55% to 61% in the ELS tests. However, the same unstable behaviour was obtained due to the adhesive failure [25] as shown in Fig. 15. On the other hand, testing at high temperatures slightly reduces the values of both $\mathcal{G}_{in}$ and $\mathcal{G}_c$ (having a maximum reduction of 25%) in the case of DCB specimens, while it increases the fracture toughness of the ELS specimens (see Fig. 13).

In general, the exposure to high temperatures decreases the maximum cohesive stress. On the contrary, this value increases when testing at freezing temperatures. Specifically, for the non-aged DCB specimens, temperature affects the initiation traction stress, i.e. for the specimens tested at 80 °C, the maximum traction stress was reduced by 11% compared to the same result at RT. On the contrary, the maximum stress increased by a 10% in the case of specimens tested at −55 °C,

independently on the ageing condition. Regarding the wet-aged DCB specimens, the maximum traction stress of A1/80/W and A2/80/W DCB specimens decreases around 9% of the maximum traction value at room temperature (48 MPa and 30 MPa for A1/RT/W and A2/RT/L respectively). In contrast, the maximum traction stress of specimens exposed to freezing temperatures increases to a value of 54 MPa in the case of A1/-55/W. Concerning the mode II specimens, the maximum shear stress τ_0 increases by 5% and 14%, for A1 and A2 non-aged specimens when the temperature decreases from RT to −55 °C. While freezing temperatures on wet-aged ELS specimens cause an increase in the value of τ_0 by a 5% and 21% in A1 and A2 materials, respectively.

Exposing the composite bonded joints to aggressive environmental changes (temperature and humidity) for a long time has a great effect on the fracture response [2,34–38]. Therefore, comparing the behaviour of the specimens exposed to accelerated ageing to the non-aged specimens for both A1 and A2 materials leads to better understanding of the environmental effects over time. It is noticed that the fracture toughness of the adhesive (i.e. the area under the CL) degraded significantly, as shown in Fig. 14. For the DCB results, the fracture toughness of the wet-aged specimens tested at RT degrades around 40% and 70% compared to the non-aged A1 and A2 counterparts, respectively. This reduction of the fracture toughness is related to the adhesive failure observed on both sides of the fractured surfaces of the DCB wet-aged specimens [24], see Fig. 15. As discussed by Abdel-Monsef et al. [24], the adherend delamination is guided by the fracture toughness of the epoxy resin, which is lower than the fracture toughness of the adhesive film [39,40]. Moreover, the maximum traction stress (σ_0) is reduced, e.g. σ_0 of the wet-aged specimens tested at RT gets reduced a 12% and 40% compared to the non-aged values for A1 and A2 configurations, respectively. Regarding the effect of ageing on the ELS test results, it is noticed that wet-ageing has a significant influence on the fracture properties of the adhesive interface. The fracture toughness degraded by a 26% and 78% the non-aged ELS specimens values for A1 and A2 configurations, respectively.

5. Conclusions

In the current work, the influence of temperature and ageing on the cohesive laws of composite bonded joints in mode I and mode II was studied for two types of secondary bonded composite joints. The composite bonded joints were tested using DCB and ELS test configurations for mode I and mode II, respectively, under various

temperatures (−55 °C, RT and 80 °C) and ageing conditions (wet-aged and non-aged). From the analysis of the results, it can be concluded the shape of the cohesive law should not pre-assumed as it changed with the environmental conditions.

Exposure to the different environmental conditions mentioned above was found to affect the shape of the cohesive laws of the studied composite bonded joints. It is observed that ageing mainly affects the cohesive law by reducing the fracture energy while the exposure to high temperature or freezing temperature changes the shape of the cohesive law.

Few research studies predefine the shape of the cohesive law and scale the area under the cohesive law with environmental conditions depending on the measured cohesive parameters. The main novelty of this work is that the environmental effects on the cohesive law are analysed from a full experimental point of view, without considering a predefined shape for the CL. Thus, the effect of the main driving damage mechanisms on the shape of the cohesive law, which change depending on the environmental conditions, is captured. This analysis constitutes an essential step in the definition of cohesive numerical models that take into account environmental effects, since taking into account the shape of the cohesive law leads to more accurate prediction of the bond behaviour [41]. It is found that bilinear/trilinear shape is the best fit of the mode I cohesive laws, as seen in the results in Figs. 5 to 8. While in the case of mode II, the cohesive laws are characterized by a wide initial plateau, see Figs. 9 to 12. Thus, a trapezoidal shape combined with a linear softening is the shape that best fits the mode II cohesive laws of the adhesives tested.

CRediT authorship contribution statement

S. Abdel-Monsef: Conceptualization, Methodology, Investigation, Writing – original draft. **J. Renart:** Supervision, Methodology, Writing – review & editing. **L. Carreras:** Methodology, Writing – review & editing. **P. Maimí:** Methodology, Writing – review & editing. **A. Turon:** Supervision, Methodology, Writing – review & editing.

Declaration of competing interest

The authors declare that they have no known competing financial interests or personal relationships that could have appeared to influence the work reported in this paper.

Acknowledgements

Appendix A. Supplementary data

Supplementary material related to this article can be found online at https://doi.org/10.1016/j.compositesa.2021.106798.

References

[1] Fernandes R, de Moura M, Moreira R. Effect of temperature on pure modes I and II fracture behavior of composite bonded joints. Composites B 2016;96:35–44.

[2] Fernandes R, De Moura M, Moreira R. Effect of moisture on pure mode I and II fracture behaviour of composite bonded joints. Int J Adhes Adhes 2016;68:30–8.

[3] Amancio-Filho S, Dos Santos J. Joining of polymers and polymer–metal hybrid structures: recent developments and trends. Polym Eng Sci 2009;49(8):1461–76.

[4] Banea M, da Silva LF. Adhesively bonded joints in composite materials: an overview. Proc Inst Mech Eng L: J Mater: Des Appl 2009;223(1):1–18.

[5] Budhe S, Banea M, De Barros S, Da Silva L. An updated review of adhesively bonded joints in composite materials. Int J Adhes Adhes 2017;72:30–42.

[6] Liu S, Cheng X, Zhang Q, Zhang J, Bao J, Guo X. An investigation of hygrothermal effects on adhesive materials and double lap shear joints of CFRP composite laminates. Composites B 2016;91:431–40.

[7] Zhang Y, Vassilopoulos AP, Keller T. Effects of low and high temperatures on tensile behavior of adhesively-bonded GFRP joints. Compos Struct 2010;92(7):1631–9.

[8] Adams R, Coppendale J, Mallick V, Al-Hamdan H. The effect of temperature on the strength of adhesive joints. Int J Adhes Adhes 1992;12(3):185–90.

[9] Adams R, Mallick V. The effect of temperature on the strength of adhesively-bonded composite-aluminium joints. J Adhes 1993;43(1–2):17–33.

[10] Gustafson PA, Waas AM. Experiments and cohesive zone model parameters for T650/AFR-PE-4/FM680-1 at high temperatures. J Aerosp Eng 2011;24(3):285–97.

[11] Goglio L, Rezaei M. Effect of environmental exposure on the fracture properties of an epoxy adhesive. J Adhes 2013;89(11):807–21.

[12] LaPlante G, Lee-Sullivan P. Moisture effects on FM300 structural film adhesive: Stress relaxation, fracture toughness, and dynamic mechanical analysis. J Appl Polym Sci 2005;95(5):1285–94.

[13] Ray B. Temperature effect during humid ageing on interfaces of glass and carbon fibers reinforced epoxy composites. J Colloid Interface Sci 2006;298(1):111–7.

[14] Banea M, Silva Ld, Campilho R. Effect of temperature on tensile strength and mode I fracture toughness of a high temperature epoxy adhesive. J Adhes Sci Technol 2012;26(7):939–53.

[15] Mohan J, Ivanković A, Murphy N. Effect of prepreg storage humidity on the mixed-mode fracture toughness of a co-cured composite joint. Composites A 2013;45:23–34.

[16] Markatos D, Tserpes K, Rau E, Brune K, Pantelakis S. Degradation of mode-I fracture toughness of CFRP bonded joints due to release agent and moisture pre-bond contamination. J Adhes 2014;90(2):156–73.

[17] Tserpes K, Markatos D, Brune K, Hoffmann M, Rau E, Pantelakis S. A detailed experimental study of the effects of pre-bond contamination with a hydraulic fluid, thermal degradation, and poor curing on fracture toughness of composite-bonded joints. J Adhes Sci Technol 2014;28(18):1865–80.

[18] Budhe S, Rodríguez-Bellido A, Renart J, Mayugo J, Costa J. Influence of pre-bond moisture in the adherents on the fracture toughness of bonded joints for composite repairs. Int J Adhes Adhes 2014;49:80–9.

[19] Banea M, da Silva LF, Campilho R. Temperature dependence of the fracture toughness of adhesively bonded joints. J Adhes Sci Technol 2010;24(11–12):2011–26.

[20] Banea M, Da Silva L, Campilho R. Mode I fracture toughness of adhesively bonded joints as a function of temperature: experimental and numerical study. Int J Adhes Adhes 2011;31(5):273–9.

[21] Banea M, Da Silva L, Campilho R. Mode II fracture toughness of adhesively bonded joints as a function of temperature: experimental and numerical study. J Adhes 2012;88(4–6):534–51.

[22] ISO 25217: 2009. Adhesives–determination of the mode I adhesive fracture energy of structural adhesive joints using double cantilever beam and tapered double cantilever beam specimens. Br Stand 2009.

[23] ISO 15114: 2014. Fibre-reinforced plastic composites-determination of the mode ii fracture resistance for unidirectionally reinforced materials using the calibrated end-loaded split (C-ELS) test and an effective crack length approach. 2014, ISO Genève.

[24] Abdel-Monsef S, Renart J, Carreras L, Maimí P, Turon A. Effect of environmental conditioning on pure mode I fracture behaviour of adhesively bonded joints. Theor Appl Fract Mech 2020;102826.

[25] Abdel-Monsef S, Renart J, Carreras L, Turon A, Maimí P. Effect of environment conditioning on mode II fracture behaviour of adhesively bonded joints. Theor Appl Fract Mech 2021;112:102912.

[26] Abdel Monsef S, Ortega A, Turon A, Maimí P, Renart J. An efficient method to extract a mode I cohesive law for bonded joints using the double cantilever beam test. Composites B 2019;178:107424.

[27] Abdel Monsef S, Pérez-Galmés M, Renart J, Turon A, Maimí P. The influence of mode II test configuration on the cohesive law of bonded joints. Compos Struct 2019;111689.

[28] ABAQUS. ABAQUS 6.14 user's manual. 2014.

[29] Arenas JM, Ocaña R, Alía C, Narbón JJ, Islán M. Fracture energy in structural adhesive joints of composite-aluminum under adverse environments conditions. J Adhes Sci Technol 2014;28(2):201–14.

[30] Banea MD, da Silva LF. Mechanical characterization of flexible adhesives. J Adhes 2009;85(4–5):261–85.

[31] Crocombe A, Hua Y, Loh W, Wahab M, Ashcroft I. Predicting the residual strength for environmentally degraded adhesive lap joints. Int J Adhes Adhes 2006;26(5):325–36.

[32] Quan D, Urdániz JL, Rouge C, Ivanković A. The enhancement of adhesively-bonded aerospace-grade composite joints using steel fibres. Compos Struct 2018;198:11–8.

[33] da Silva LF, De Magalhães F, Chaves F, De Moura M. Mode II fracture toughness of a brittle and a ductile adhesive as a function of the adhesive thickness. J Adhes 2010;86(9):891–905.

[34] Dawood M, Rizkalla S. Environmental durability of a CFRP system for strengthening steel structures. Constr Build Mater 2010;24(9):1682–9.

[35] Li S, Ren HT, Lu YY, Shi MH. Environmental degradation of carbon fiber reinforced polymer (CFRP) and steel bond subjected to hygrothermal aging and loading. In: Materials science forum, Vol. 675. Trans Tech Publ; 2011, p. 559–62.

[36] Nguyen T-C, Bai Y, Zhao X-L, Al-Mahaidi R. Durability of steel/CFRP double strap joints exposed to sea water, cyclic temperature and humidity. Compos Struct 2012;94(5):1834–45.

[37] Yong-xin Y, Qing-rui Y, Fu-ming P. Experimental research on bond behavior of CFRP to steel. In: Int. symp. bond behav. FRP struct.. 2005, p. 419–24.

[38] Roy A, Gontcharova-Benard E, Gacougnolle J-L, Davies P. Hygrothermal effects on failure mechanisms of composite/steel bonded joints. In: Time dependent and nonlinear effects in polymers and composites. ASTM International; 2000.

[39] Costa J, Mahdi S, Renart J, Álvarez J, de la Torre M, et al. Quality assessment of bonded joints for repair purposes with adhesive films and laminating resins. In: International conference on composite materials, Vol. 17. 2009.

[40] Costa J, Renart J, Batista Y, Mahdi S, Rodríguez-Bellido A. Detailed investigation of bonded joints for composite repairs. In: Proceedings of 18 th international conference on composite materials. 2011, p. 21–6.

[41] Campilho RD, Banea MD, Neto J, da Silva LF. Modelling adhesive joints with cohesive zone models: effect of the cohesive law shape of the adhesive layer. Int J Adhes Adhes 2013;44:48–56.